MLF Experimental Report	提出日 Date of report 2013/05/20
実験課題番号 Project No. 2014P0102 実験課題名 Title of experiment Strength of Materials and Related Engineering 実験責任者名 Name of principal investigator Y. Tomota 所属 Affiliation Ibaraki University	装置責任者 Name of responsible person K. Aizawa 装置名 Name of Instrument/（BL No.） TAKUMI (BL19) 利用期間 Dates of experiments 2014: 5/8-10, 6/21, 2015: 4/27-28 (Topic A), 2014: 5/31-6/3 (Topic B), 2014: 5/22-26, 12/12-15 (Topic C)

1．研究成果概要（試料の名称、組成、物理的・化学的性状を明記するとともに、実験方法、利用の結果得られた主なデータ、考察、結論、図表等を記述してください。

Outline of experimental results (experimental method and results should be reported including sample information such as composition, physical and/or chemical characteristics.

Overall outline of the experimental results in the project

This project includes three topics, *i.e.*, (1) Mg based synchronized LPSO alloys (Topic A), (2) Commercial superconductor composite materials (Topic B), and (3) Advanced steels (Topic C). The main results obtained in these three topics are described in order.

Topic A： Crystal structure and mechanical properties of Mg based synchronized LPSO alloys

Following the experiments in the last fiscal year, deformation mechanism of Mg based LPSO alloys were studied. Mechanical properties of two-phase alloys (Mg97Zn1Y2) composed of LPSO phase and alpha Mg phase are different depending on manufacturing process. For example, the yield strength of a cast sample was 111 MPa whereas that of an extruded sample 263 MPa. Hence, in this year, in situ neutron diffraction measurements were performed for these two kinds of alloys, cast and extruded.

The results obtained in the cast alloy are presented in Fig. 1. The twinning in the alpha Mg phase and

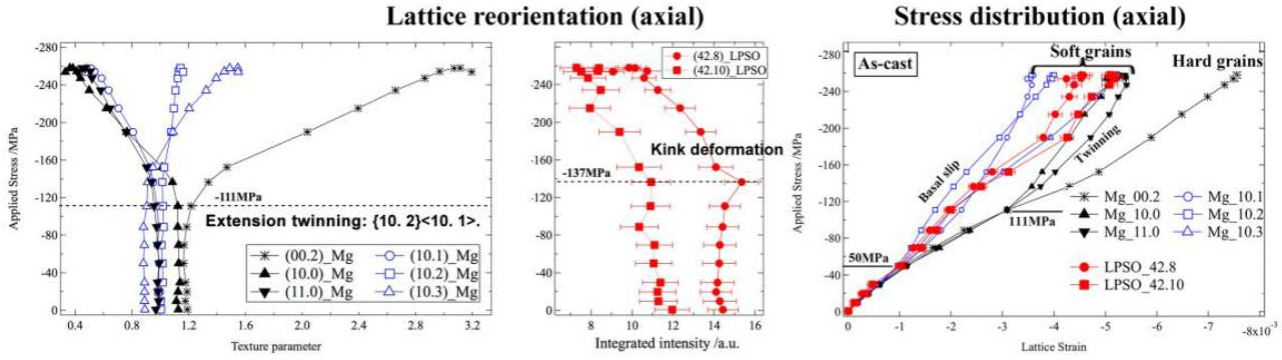

Fig. 1 changes in lattice strain and crystal orientation in the axial direction with compressive deformation in the cast two-phase LPSO alloy.

kinking in the LPSO phase result in changes of hkl diffraction intensities caused by crystal rotation. The critical stress corresponding to the onset of plastic deformation by each mode was determined from reorientation of grains and lattice strains. Figure 2 shows the critical stress for each deformation mode as a function of the external compressive stress. The LPSO phase deforms plastically with the basal plane slip of the alpha Mg phase in the cast alloy, whereas the alpha Mg phase deforms preferentially followed by the increase of stress in the LPSO; that is, the LPSO phase plays hard second phase in the extruded alloy. Then, the critical stress of -50 MPa for the onset of slip deformation of the basal plane in the cast alloy is strengthened up to -263 MPa in the extruded alloy. It is, therefore, concluded that the kink bands introduced in the LPSP phase hinder plastic deformation so as to exhibit kink-strengthening.

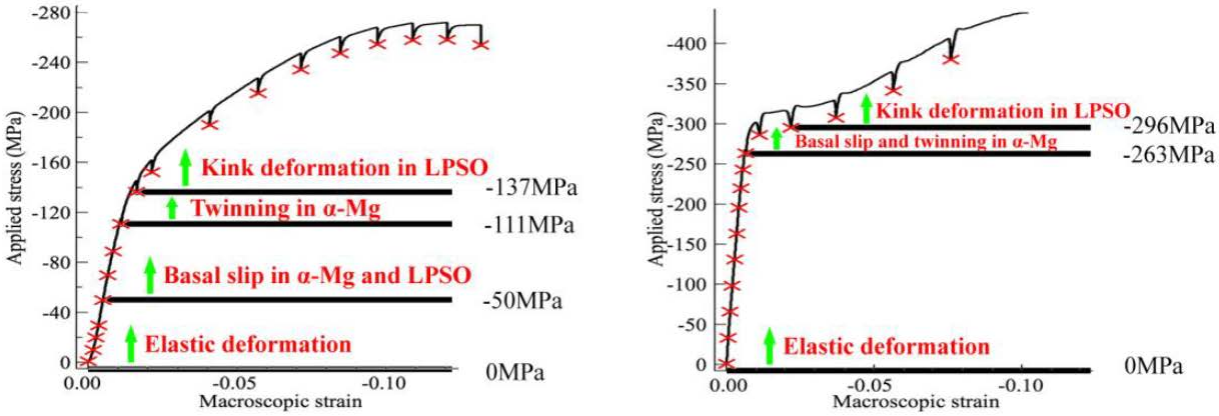

Fig. 2 Compressive stress-strain curves for the cast two-phase alloy (a) and the extruded two-phase alloy (b). in which the deformation modes estimated from the in situ neutron diffraction results were inserted.

Topic B: Influence of stress and/or strain on commercial super conductive composite materials

Strains under tensile loading at cryogenic temperatures were measured for Nb_3Sn Rutherford cables, the cross section of which was depicted in Fig. 3. In the last year, the composite after cyclic bending strain treatment was examined, but the sample of this year was not treated. As shown in Fig. 4, it was found that larger residual strains were observed in the composite (cable) after bent treatment, which was similar to the case of the element wire. It was also found the strains of the composite and element wires were different from each other as was presented in Fig. 5. This is probably due to the twist wire conductors. Using this conductor component, the development of 25T super conductor magnet without coolant was finished. In March, 2015, the generation of 14T magnetic field was successfully realized and further 24.6T by combining with high temperature super conductor insert.

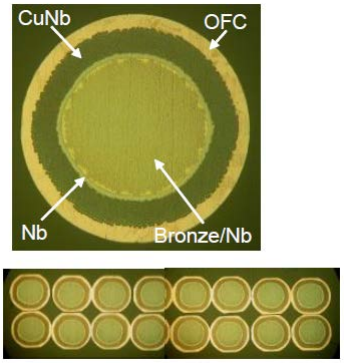

Fig. 3 Cross section of the CuNb Rutherford cable (above) and that of element wires (b).

The experiments planned in Jan. 24 – 27 for strain measurement

必要に応じて、A4 サイズの用紙に続きを記入して下さい。
Please use A4-size papers for further reporting, if necessary.

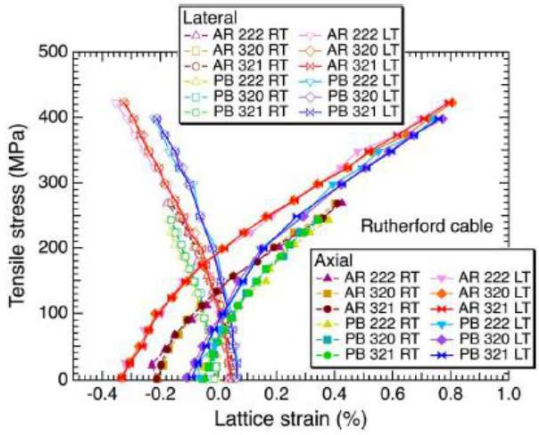

Fig. 4 Strains of Nb_3Sn phase in the CuNb Rutherford cable.

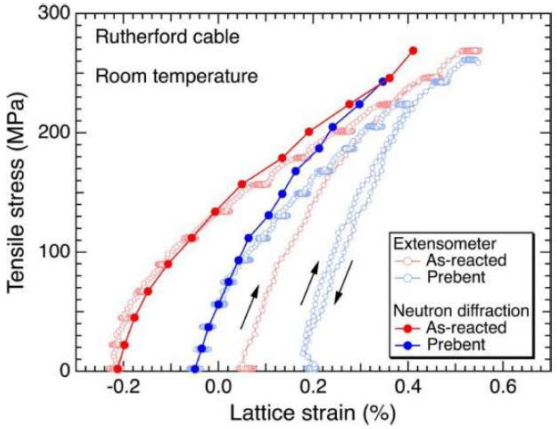

Fig. 5 Overall stress-strain properties a and strains of Nb_3Sn phase in the CuNb Rutherford cable.

of Nb3Sn coil at cryogenic temperatures (Tohoku Univ.) and those in Feb. 4 – 6 for low temperature tensile test for high temperature super-conductor tape, RE-Ba-Cu-O were cancelled due to the J-PARC accident.

Topic C: Development of advanced steels using in situ neutron diffraction

Three kinds of experiments were conducted.

The first one was in situ neutron diffraction measurements during tension-compression Baushinger effect tests and low cycle fatigue tests for Fe-Cr-Ni alloys aiming at study the effect of deformation induced martansite transformation, Fe-Si alloys and Fe-Ni-C alloys to investigate work hardening mechanism, and

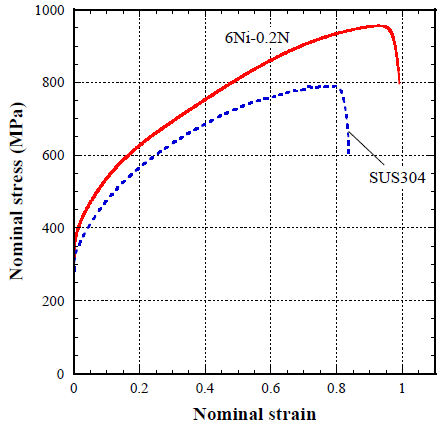

Fig. 5 Stress-strain curves for 6Ni-0.2N steel steel.

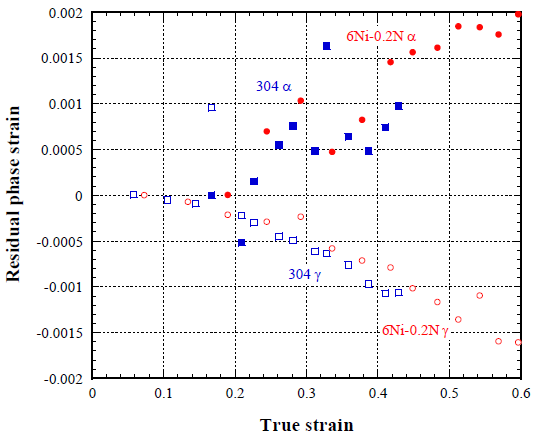

Fig. 6 Residual phase strains in 6Ni-0.2N and SUS 304 steel and SUS 304.

必要に応じて、A4 サイズの用紙に続きを記入して下さい。
Please use A4-size papers for further reporting, if necessary.

pearlite steels to study cyclic hardening or softening behavior. It was new trials to employ line profile analysis to make clear the deformation mechanisms of these steels, which could not be performed by any other techniques. As one typical results, Figures 5 and 6 show the results for 6Ni-0.2N and SUS 304 steels by Tsuchida et al. (Hyogo Pref, Univ.), where stress-strain curves were shown in Fig. 5 to show different behaviors. As seen, both of tensile strength and elongation were larger in 6Ni-0.2n steel. It is noted that work hardening rate becomes larger in the latter stage of tensile deformation in 6Ni-0.2N steel. Figure 6 shows the residual phase strains in austenite and ferrite phases. The difference in phase strains between these two constituent phases are larger in 6Ni-0.2N steel than SUS 304 steel, which indicate higher work hardening in the former steel. It is concluded that the reasons of better strength-elongation balance in 6Ni-0.2 steel include macroscopically higher work-hardening stemmed from microscopically larger phase stresses due to higher strength of martensite induced during deformation.

The second is concerning how to evaluate quantitatively microstructural parameters. The neutron diffraction measurements were performed for swaged samples of Fe-Ni-C(-Al) steel, duplex stainless steel and low alloyed TRIP steels. As has already been made clear, neutron diffraction method is superior compared with other method like X-ray diffraction or SEM/EBSD methods to obtain the bulk information on texture. In the present beam time, texture in two-phase alloys were determined to construct the ODF map individually for each component phases. A typical example obtained was presented in Fig. 7 for the case of martensite/austenite layered sample. As seen,

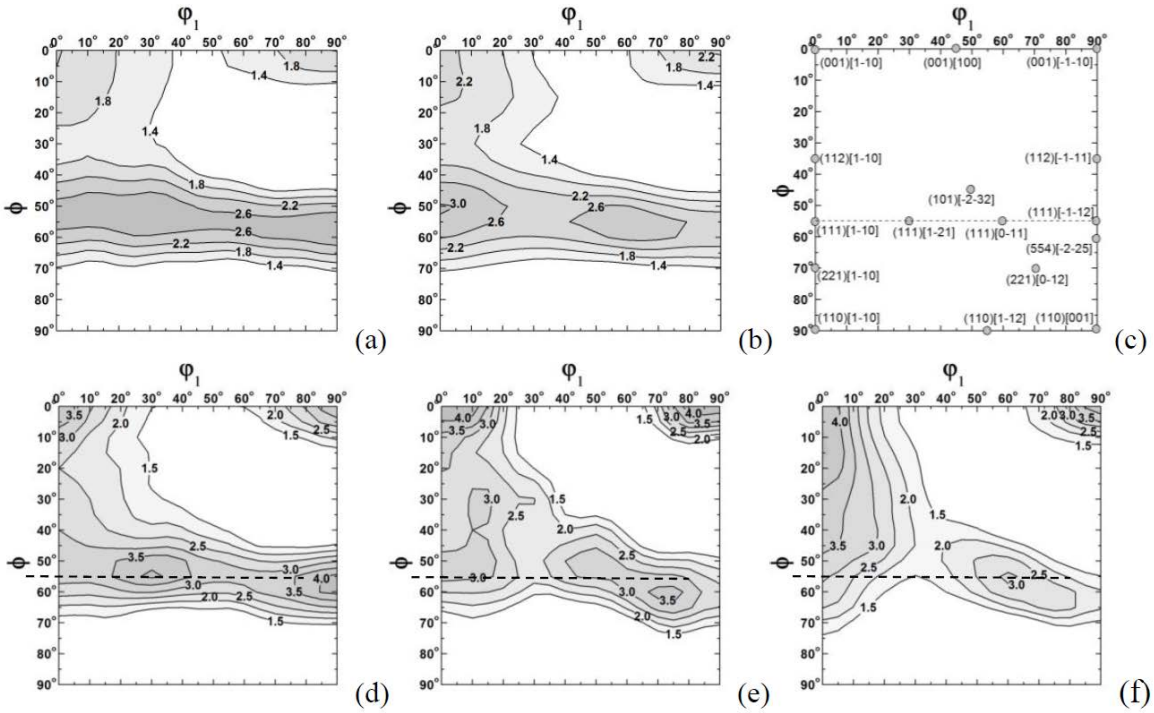

Fig. 7 Orientation distribution function (ODF) map determined by neutron diffraction: (a-d) martensite single phase steel, (d-f) martensite steel/austenite steel clad materials, where the effect of tensile deformation on texture evolution was examined. The given strains were 0% (a. d), 5% (b. f) and (c) was the standard orientations.

必要に応じて、A4 サイズの用紙に続きを記入して下さい。
Please use A4-size papers for further reporting, if necessary.

the influence of tensile deformation on texture evolution of each component phase could be followed with changes in ODF. Recently, it has been demonstrated the determination of retained austenite volume fraction can be performed by simultaneous measurement with texture with neutron diffraction. In case of X-ray diffraction, it is insufficient to obtain bulky averaged volume fraction, where the modification concerning texture influence using the conventional method using ideal diffraction intensities was revealed insufficient. In particular, recent research and development for advanced high strength with good ductility steels contain metastable austenite phase. To evaluate the metastable austenite volume fraction is extremely important and only neutron diffraction with texture measurement can gives correct value.

The third group is concerning thermo-mechanically controlled processing. The microstructure evolution at elevated temperatures was monitored using in situ neutron diffraction measurements, including anisotropic hardening with strain aging, work hardening, recovery and recrystallization at high temperatures for Fe-Mn-C(-Nb) alloys and austenitic steels of Fe-33Ni alloy and SUS 310 steel. Tempering behavior for a tool steel (SKD: martensite steel) was also monitored how dislocation density and arrangement change with tempering and the obtained results were discussed comparing the changes in hardness (mechanical properties). Here, the determination of dislocation density with tensile deformation at room temperature and subsequent annealing for the same sample of SUS 310 was presented in Fig. 8. As is observed, the CMWP model fitting to diffraction profiles enables us to determine the decrease in dislocation density with increasing of annealing temperature. The experiment was made using one tensile specimen using tensile tester equipped with a image furnace to track work hardening, recovery and recrystallization for the identical gauge volume. To be noted here is the CMWP fitting method provides not only total dislocation density but also that for individual <hkl> oriented family grains (see the right figure). The development of this kind of measurements is extremely valuable to develop advanced processing for new steels.

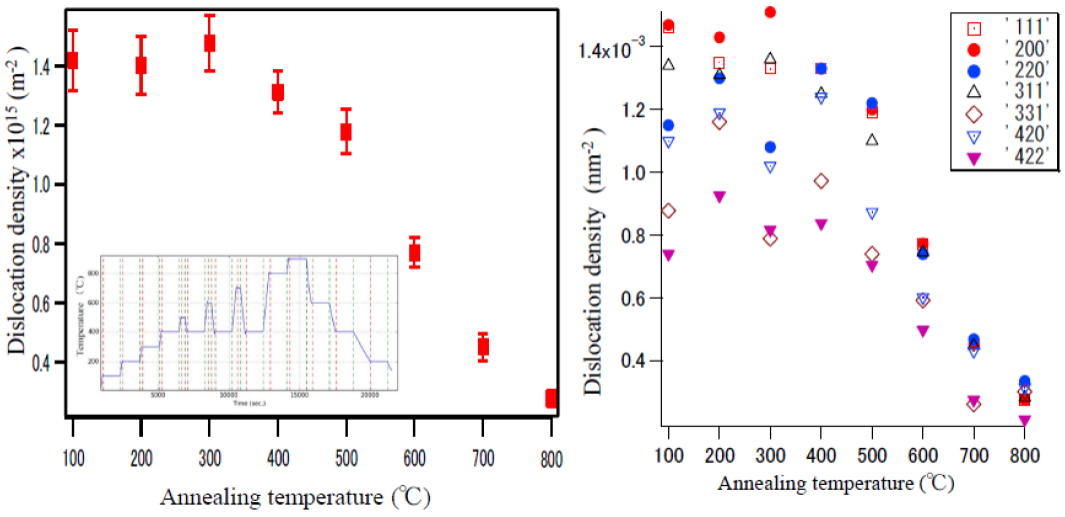

Fig. 8 Change in dislocation density with annealing after tensile deformation of 40% at RT for SUS 310 steel (left) and those for individual <hkl> family grains determined using the CMWP fitting for neutron diffraction profiles.